NANO LETTERS

2007
Vol. 7, No. 2
458−463

Electrospun Light-Emitting Nanofibers

José M. Moran-Mirabal,*,† Jason D. Slinker,‡ John A. DeFranco,‡ Scott S. Verbridge,§ Rob Ilic,† Samuel Flores-Torres,|| Héctor Abruña,|| George G. Malliaras,‡ and H. G. Craighead†

School of Applied and Engineering Physics, Department of Materials Science and Engineering, Physics Department, and Department of Chemistry and Chemical Biology, Cornell University, Ithaca, New York 14853

Received November 28, 2006; Revised Manuscript Received January 9, 2007

ABSTRACT

We have electrospun light-emitting nanofibers from ruthenium(II) tris(bipyridine)/polyethylene oxide mixtures. The electroluminescent fibers were deposited on gold interdigitated electrodes and lit in a nitrogen atmosphere. The fibers showed light emission at low operating voltages (3-4 V), with turn-on voltages approaching the band gap limit of the organic semiconductor. Because of the fiber size, emission from electrospun light-emitting nanofibers is confined to nanoscale dimensions, an attractive feature for sensing applications and lab-on-a-chip integration where highly localized excitation of molecules is required.

Light-emitting sources with constrained dimensions have received much attention because of their importance in sensing and lab-on-a-chip applications.[1−5] The ability to shrink the size of an illumination source and couple it with on-chip detection mechanisms can enable the production of fully packaged, functional devices that operate without the need of external optics. This can, in turn, enhance the sensitivity and improve the signal-to-noise ratio of detected fluorescence by limiting the number of interfaces through which the emitted light has to propagate.[6] State of the art lab-on-a-chip devices use external illumination sources, such as lasers or light emitting diodes (LEDs).[2,3,6] Even though LEDs are relatively inexpensive and can have submillimeter size, they are still much larger than the typical micro- or nanofluidic device and have to be mounted outside of the sensing region. Some attempts have been made at fabricating on-chip point sources that can be coupled to micro- and nanofluidic devices.[1,2,5,7] However, these point sources are usually much larger than the fabricated devices, can be expensive to fabricate, or do not emit in the visible spectrum.

Light-emitting devices based on organic semiconductors have been demonstrated as efficient sources with characteristics that make them attractive for flat panel displays, lighting, and sensing applications.[1,3,8−13] For many of these materials, the organic semiconductor can be deposited directly from solution, thus affording ease of fabrication. Within the class of solution processable organic electroluminescent materials, ionic transition metal complexes (iTMCs) have emerged as materials that allow the fabrication of efficient, single-layer light-emitting devices employing air-stable electrodes.[14−23] These features are a consequence of the operational mechanism of iTMC light-emitting devices, which is similar to that of polymer light-emitting electrochemical cells.[24−28] In these materials, ionic space charge effects lead to both enhancement of electronic charge injection (enabling the use of air-stable electrodes[17]) and a light emission profile confined to a thin region of the active area between the electrodes. These characteristics make organic light-emitting devices, and in particular iTMC devices, attractive candidates for on-chip light sources. In this sense, having a light-emitting nanofiber based on an iTMC could provide a point source emission profile, with the axial dimension restricted by the iTMC operational mechanism and the radial dimension given by the diameter of the nanofiber.

Electrospinning is a well-developed electrohydrodynamic method used to produce micro- and nanofibers from a variety of dissolved materials without the need of expensive fabrication methods.[29−31] In a typical electrospinning setup, high voltage is applied to a droplet of the solution that rests on a sharp conducting tip. As a result of molecular ionization and charge redistribution, a Taylor cone is formed and a jet of the solution is extracted.[32] The formed jet is then accelerated by the electric field and collected on a grounded substrate. When a volatile solvent is used, in-flight solvent evaporation occurs, hardening the fibers composed of the dissolved material, which are deposited on the substrate. With this technique, fibers have been electrospun from a wide variety of polymers.[33−35] Fibers containing biomolecules (e.g., enzymes[36] and DNA[37,38]) and particles (e.g., viruses,[39] carbon

* Corresponding author: jmm248@cornell.edu.
† School of Applied and Engineering Physics.
‡ Department of Materials Science and Engineering.
§ Physics Department.
|| Department of Chemistry and Chemical Biology.

10.1021/nl062778+ CCC: $37.00
Published on Web 01/23/2007

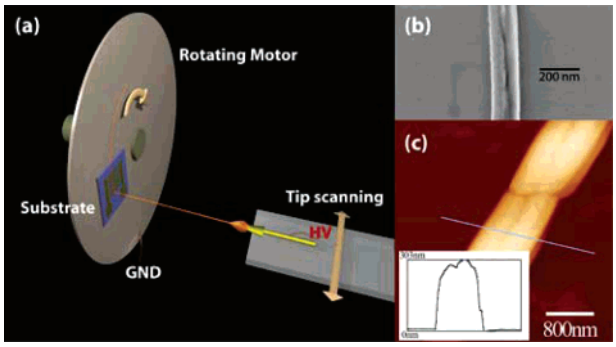

Figure 1. Electroluminescent nanofibers can be easily produced with electrospinning. (a) Schematic of the electrospinning setup used to deposit the fibers on the substrate. Fibers are oriented by the rotating motion of the substrate. Oriented fibers are obtained over a wide area by scanning the tip sideways. (b) Scanning electron micrograph of an electrospun nanofiber with a diameter of 150 nm. (c) Atomic force micrograph of an electrospun nanofiber with ~300 nm height.

nanotubes,[40,41] and CdSe quantum dots[42]) imbedded in a carrier polymer, have also been produced. An advantage of electrospinning is that the fibers can be deposited over trenches or on conducting electrodes, facilitating mechanical, optical, and electrical interrogation of the fiber properties.[43] We have used the electrospinning technique to deposit fibers containing electroluminescent iTMCs imbedded in a polymer electrolyte on interdigitated electrodes to produce point illumination sources.

The solution used for electrospinning was made by dissolving ruthenium(II) tris(bipyridine) ($[Ru(bpy)_3]^{2+}(PF_6^-)_2$) in dry acetonitrile at 50 mM concentration. The solution was then filtered through a 450 nm polycarbonate membrane to remove large particle impurities. Poly(ethylene oxide) (PEO, 10^6 Da MW, Sigma) was subsequently added as a carrier polymer at 1−3% weight/weight ratio (10−30 nM concentration of PEO polymer). The variation in the PEO percentage allowed tuning the viscosity of the electrospinning solution which affected the size of the deposited fibers. In addition to the ease of electrospinning allowed by the material properties of PEO, it has been also shown that PEO can have a positive impact on the electrical characteristics of ruthenium complex devices. Lyons et al. demonstrated improved response times of Ru devices blended with PEO due to enhancement of the ionic conductivity.[44] In the past, other polymers (e.g., poly(methyl methacrylate), polycarbonate, and polystyrene) have been also blended with metal complexes and used to make thin-film light-emitting devices. Rudmann and Rubner have reported that such blends can increase device lifetimes and improve film quality.[45] Such polymers blended with Ru metal complexes could also be used to form electrospun light-emitting nanofibers. The fibers used for the experiments described below were electrospun using a microfabricated tip coated with a thin gold layer in a setup as depicted in Figure 1a. The voltage used for electrospinning was varied between 8 and 10 kV, and the tip-to-substrate distance was kept between 25 and 40 mm. The resulting fibers had diameters that ranged from 150 nm (smallest fibers produced with 1% PEO solution) to several micrometers (largest fibers from 3% PEO solution), as confirmed by scanning electron microscopy (Figure 1b) and atomic force microscopy profiles (Figure 1c). Some fibers electrospun with 3% PEO content showed phase separation between the polymer and the transition metal complex.

The silicon substrates used to collect the fibers had 300−600 nm thermal oxide as an insulating layer with micropatterned gold interdigitated electrodes (IDEs, Figure 1a) on top. Multiple fibers were electrospun onto IDEs with interelectrode spacing of either 500 nm or 5 μm. The electrospun fibers were lit by applying a dc bias across the IDEs in a dry nitrogen atmosphere. In this arrangement, each fiber region spanning the interelectrode gap between a positive and negative electrode could potentially produce a local light-emission zone (though not all did in practice). Thus, there were several emission zones for the overall IDE device. In all experiments performed, the current passing through the device was monitored as the voltage was ramped up/down and light emission occurred. An important remark is that because each device contained more than one fiber on top of the IDEs, the current recorded was the total current passing through all the fibers deposited on the device. The substrates were imaged on an IX-71 inverted microscope (Olympus), and light emitted from the electrospun luminescent nanofibers (ELFs) was collected through a 50×/0.5 NA LMPlanFl Objective (Olympus) and a D620/60 m emission filter (Chroma). The electroluminescence spectrum for the fibers was captured with a calibrated Ocean Optics S2000 spectrometer. Pictures and video recordings of the emitted light were acquired using a Cascade512 CCD camera (Roper Scientific). Videos recorded from the experiments were analyzed with a custom program written in Matlab (The Mathworks) to extract intensity data form each of the emission zones in a fiber. The light emission was averaged across representative individual light-emitting regions as noted below.

In Figure 2, we demonstrate the highly localized nature of the emission from ELFs. Panels a−c of Figure 2 show the emission from a 1.1 μm thick fiber operating at 50 V on a device having a 5 μm interelectrode spacing. Emission occurs in the interelectrode gap and, in agreement with the operational mechanism described above, the emission spans only a small fraction of the entire 5 μm active region of the device. A fit of the emission profile to a Gaussian reveals a full width at half-maximum (fwhm) amplitude of 540 nm in both the axial and transverse directions in the plane of view. It may be inferred that the out-of-plane dimension is limited by the thickness of the fiber, as observed in the transverse dimension, making these three-dimensional light-emitting point sources. In the same way, panels d−f of Figure 2 show the electroluminescence from an 800 nm diameter fiber lit at 4 V on a device with 500 nm interelectrode spacing. In this case, the intensity profile is smaller—a Gaussian fit of the emitted light reveals an emission area with a 240 nm fwhm along the axial direction and a 325 nm fwhm in the transverse dimension. In reality this emission could be even smaller, as the resolution of the measurement is restricted by the diffraction limit of optical microscopy. Because the emission spectrum of the ELFs is centered at 600 nm (Figure

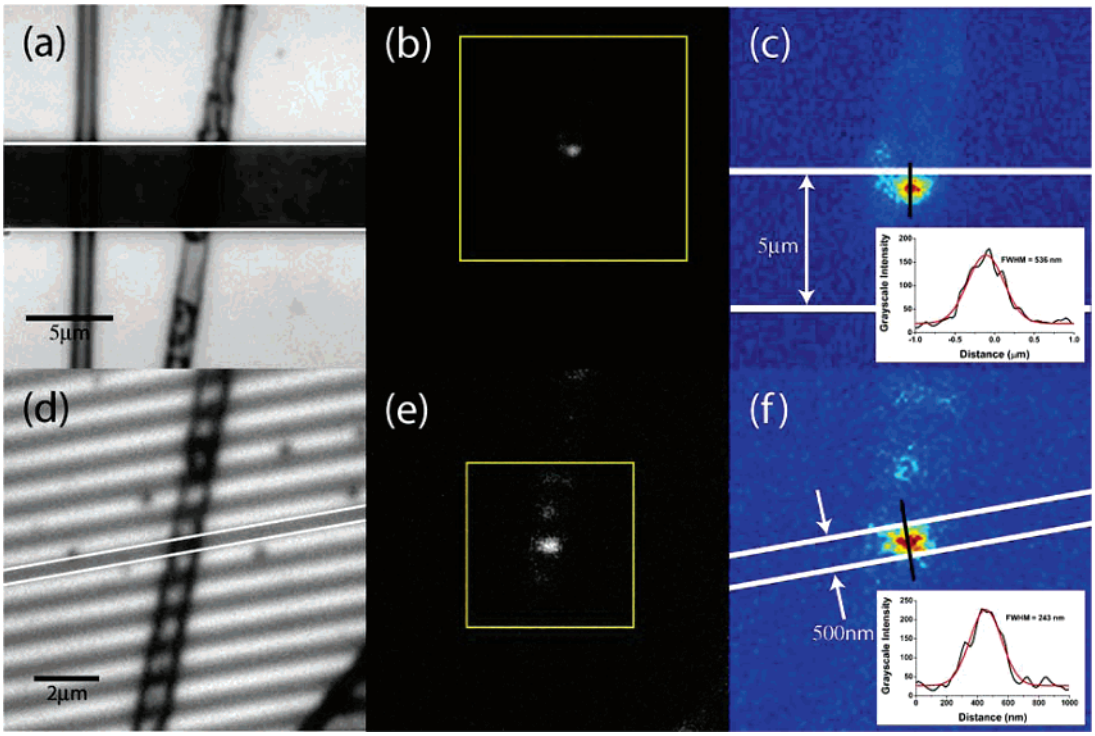

Figure 2. Electroluminescence from ELFs deposited on 5 μm and 500 nm IDEs show highly localized emission. (a) Bright field image of two fibers on a 5 μm IDE gap, outlined by white lines. (b) Emission from the right fiber imaged in (a) captured with 100 ms exposure. (c) Pseudocolor rendition of the square in (b) to illustrate intensity, white line marks the top of the IDE gap outlined in (a). Inset: intensity profile from line spanning the emission zone. Full width at half-maximum (fwhm) of the peak corresponds to 536 nm. (d) Bright field image of a single fiber spanning multiple 500 nm IDE gaps. A single gap where light emission occurs is outlined by two white lines. (e) Emission from fiber imaged in (d), captured with 100 ms exposure. Intense light emission is observed from only one IDE gap. (f) Pseudocolor rendition of square in (e), white lines mark the limits of the IDE gap outlined in (d). Inset: intensity profile from line spanning the emission zone. fwhm = 240 nm.

3), the highly localized emission restricted to a cross-sectional area of 240 × 325 nm^2 or smaller implies that the fabricated devices operate as subwavelength point sources. This confinement is similar to the smallest visible spectrum, electrically excited light-emitting sources produced to date with much more involved and expensive techniques.[5,46−48]

Figure 3 shows the typical luminescent response to an applied bias from fibers spun onto 5 μm IDEs. The voltage for fibers on these electrodes was ramped up from 0 to 130 V using 10 V increments every 15 s. The current was found to evolve with time in the periods between voltage increments, a characteristic of devices incorporating mobile ions. Light emission was detected via the CCD camera with voltages as low as 10 V and could be detected by eye in a dark room at 100 V. Light emission appeared at well-defined locations, forming emission zones with dimensions constrained ultimately by the fiber diameter and the fraction of the interelectrode spacing where recombination occurs. As the voltage was increased, more emission zones would frequently appear, resulting in multiple light sources within a fiber and a given IDE gap (Figure 3, bottom panel). Movement of the emission zones with voltage was also observed, an effect noted to occur due to changes in the relative amounts or mobilities of electrons and holes in the device.[24−27] Devices with fibers electrospun onto 5 μm IDE gaps were continuously operated under nitrogen at 100 V for a period of 10 h to assess the device stability. The emission zone imaged during this period retained 75% of its original luminance, while the current increased by 100%. Although some degradation occurs during continuous operation at high voltages, relatively long lifetimes are achieved. Higher device stability for continuous operation in air could be attained by encapsulation of the PEO light-emitting fibers or substitution of the carrier polymer.

ELFs deposited on 500 nm IDEs also emitted light when the bias was increased, with emission at voltages as low as 2.6 V. In these experiments, voltages were typically ramped between 0 and 4 V with 0.2 V increments every 15 s. Emission from fibers deposited on 500 nm IDEs did not show multiple emission zones for a given fiber in a particular electrode gap. Instead, these locations showed a homogeneous emission zone, as seen in Figure 2. For both 5 μm and 500 nm IDEs each electrospun fiber typically spanned several IDE gaps. Thus, light emission could typically be observed from more than one electrode gap in a single fiber (Figure 4). This represents an advantage when multiple light sources are required in parallel, where the emission sites would be defined by interelectrode gaps. For a particular interelectrode gap having multiple fibers spanning it, only a fraction of the fibers were found to be emitting, indicating that current preferentially passed along more conducting fiber sections. It was this fact that led to the isolated emission images shown in Figure 2.

Current−voltage ($I-V$) and luminance−voltage ($L-V$) plots were extracted from data collected from multiple fibers.

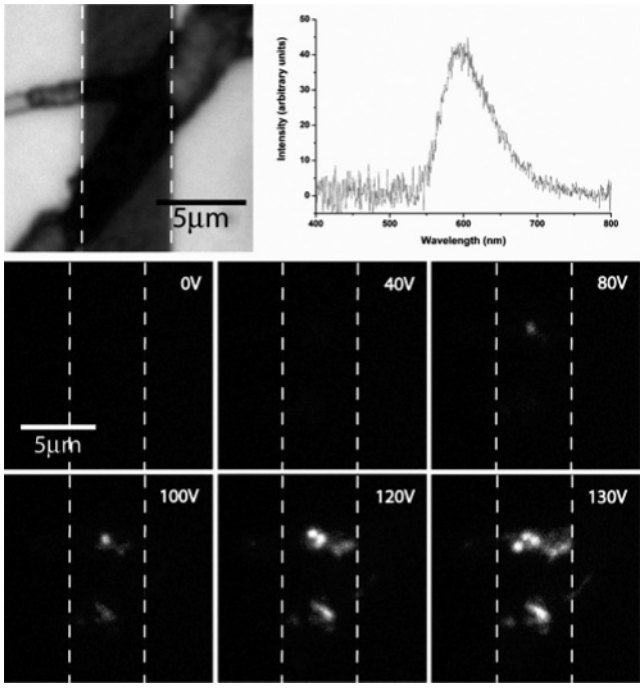

Figure 3. Light emission from fibers deposited on 5 μm spacing interdigitated electrodes (IDEs): top left, bright field image of two fibers spanning an IDE gap (dark region in background); top right, electroluminescence spectrum of light emitted from ELFs; bottom, light emission from the fibers evolves as voltage is increased. Multiple emission zones are formed within a gap for fibers spanning 5 μm IDEs.

Typical results for 5 μm and 500 nm interelectrode spacing are shown in Figure 5. In these plots, current is reported for the entire IDE array, and luminance is reported for a single, representative emission zone. For 5 μm IDEs, current and light emission followed an exponential trend, with distinguishable turn-on occurring near 10 V. By reduction of the interelectrode spacing to 500 nm, lower voltage operation was achieved (Figure 5b). For these devices, the turn-on voltage is reduced to 3.2 V, with a subsequent exponential increase of the luminance with higher voltages. Interestingly, the current shows a two-step ramping behavior, which corresponds to monopolar and bipolar injection regimes.[23] Upon application of the voltage, PF_6^- ions redistribute, leading to the onset of monopolar injection at 1.7 V. As the bias is increased, the monopoloar current continues to increase in an exponential fashion until sufficient PF_6^- motion has occurred to establish the second carrier injection at 3.2 V, initiating the onset of light emission.

To determine whether ion redistribution influences the observed current and luminance behavior in the current response from fibers electrospun onto 500 nm IDEs, we performed sequential voltage scans and followed the current and luminance. The voltage was ramped up, held at 4 V for 10 min (allowing the current to reach a steady state), and then ramped down and held at 0 V for 10 min. If the observed behavior was due to ion-assisted injection, the downward voltage ramp should reveal new current features as significantly more ionic space charge should be concentrated at the contacts. It is presumed that the ion mobility is too slow for significant PF_6^- ion redistribution to occur on the downward scan on these time scales relative to the ionic distribution obtained on the 10 min of charging. Thus, for the time scales involved, the current should reflect exponential relaxation as the voltage is ramped down, similar to a conventional LED.

Figure 6 shows the experiment for one such scan for a single fiber spanning several 500 nm IDE gaps. The data reflect the total current going through the device and the luminance observed from nine individual emission zones that lit up in the field of view. The current behavior as the voltage was ramped up showed two-step operation consistent with the observations discussed above. Luminance was detectable on the ramp-up at voltages above 3.2 V. The device was maintained at 4 V for 10 min, and then the voltage was ramped down. As the voltage was ramped down, a single step was observed for the current, consistent with our hypothesis of ion-assisted injection. The luminance also decreased in an exponential fashion and could be detected with voltages as low as 2.6 V, lower than the 3.2 V turn-on voltage observed on the ramp up. This shift in the onset of emission upon the ramp up and the ramp down can be explained on the basis of ion motion. Namely, the device continues to emit on the ramp down due to the slow relaxation of ions to/from the electrodes, which continue to assist charge injection. This behavior was reproduced for subsequent scans—two-steps in the current as the voltage was

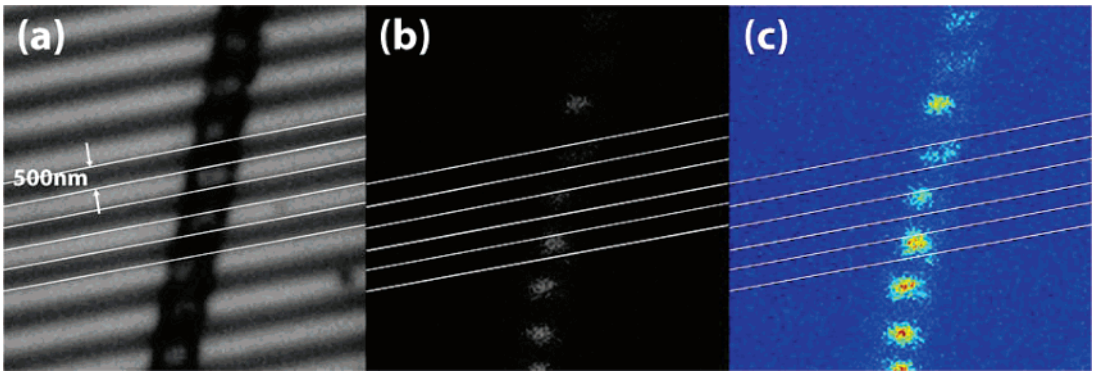

Figure 4. Light emission from multiple interelectrode gaps can be observed for a single fiber. (a) Bright field image of an electrospun fiber spanning several 500 nm IDE gaps. Electrode gaps have been outlined. (b) Emission from fiber imaged in (a) at 4 V. (c) Pseudocolor rendition of (b) for comparison of intensity in individual gaps.

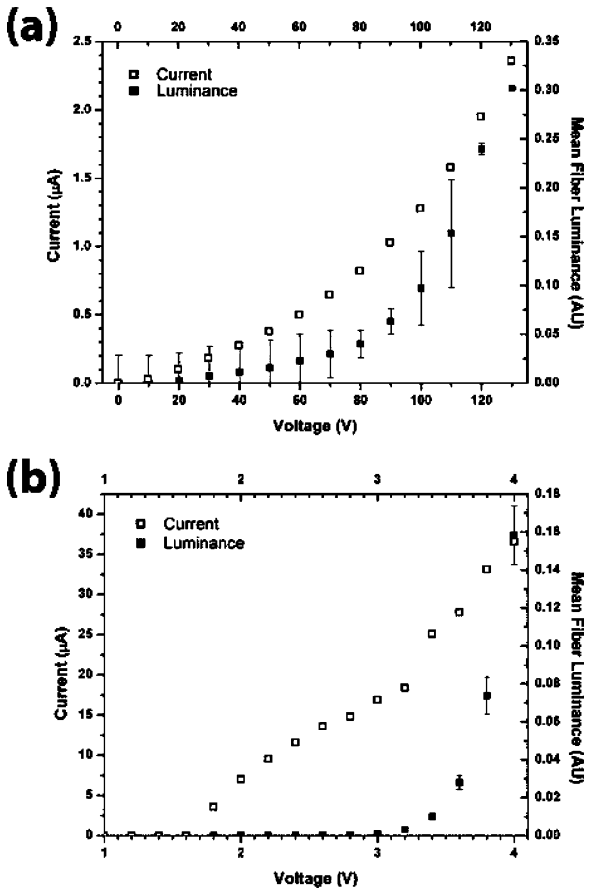

Figure 5. Current and luminance responses to an applied bias for fibers deposited on 5 μm and 500 nm IDEs. Plots represent characteristic behavior for a single emission zone. Error bars on all luminance measurements represent intensity variations along the 15 s during which each voltage was applied. (a) Current−luminance vs voltage plot for fibers on 5 μm IDEs. Exponential behavior is observed for both current and luminance. (b) Current−luminance vs voltage plot for fibers on 500 nm IDEs. Two ramping steps are observed for the current, corresponding to first and second carrier injection. Luminance shows exponential behavior.

ramped up, and exponential relaxation of the current as the voltage was ramped down. Hence, the observed $I-V$ and $L-V$ characteristics can be understood in terms of ion space charge effects.

In summary, we have shown that light-emitting fibers made from $[Ru(bpy)_3]^{2+}(PF_6^-)_2$/PEO mixtures with dimensions in the 150 nm to 5 μm range can be easily produced via the electrospinning method. Fibers were successfully lit on devices containing IDEs with interelectrode gaps of 5 μm and 500 nm. Light emission from the fibers spun on 500 nm IDEs was readily detectable with a CCD camera with voltages as low as 3.2 V and visible to the naked eye at 4 V, approaching the band gap limit for the organic semiconductor.[14] Emission from the fibers was found to be highly confined to planar regions 240 × 325 nm^2 or smaller, with imaged emission areas small enough to be limited by diffraction of the microscope. The light sources here presented could be easily integrated into micro- and nanofluidic devices for on-chip illumination. The existence of ionic transition metal complexes with emission at different wavelengths in the visible spectrum[20−22] also enables the production of nanoscopic light emitting sources that can excite multiple fluorescent tags. This, in turn, should enable the full integration of excitation and detection mechanisms on lab-on-a-chip devices.

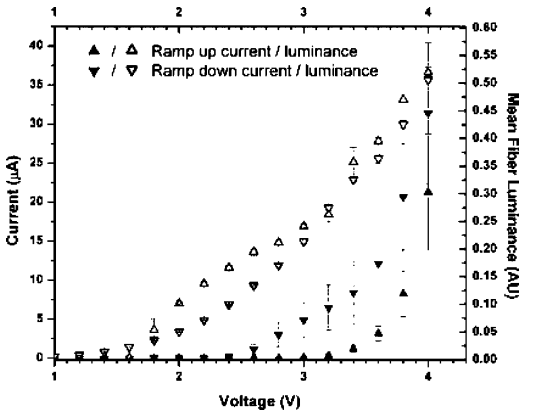

Figure 6. Ramp-up/down of the bias applied to fibers deposited on 500 nm IDEs reveals that the two steps observed in current measurements are a result of ion motion. Error bars on current measurements reflect three current readouts over the 15 s period in which the bias is applied. Error bars on luminance measurements are the standard deviation from measurements performed at nine emission zones in a single fiber.

Acknowledgment. The authors thank Christian Reccius for the use of his video-processing program and Leon Bellan for fruitful discussions. J.M.M. was supported by a CONACyT Graduate Fellowship. J.D.S. was supported by a National Science Foundation Graduate Research Fellowship. This work was supported by the New York State Office of Science, Technology and Academic Research (NYSTAR) and by the Nanoscale Science and Engineering Initiative of the National Science Foundation (NSF) under Award Number EEC-0117770. This work was performed in part at the Cornell NanoScale Facility, a member of NNIN, supported by NSF Grant ECS 03-35765. This work made use of the Cornell Center for Materials Research Shared Experimental Facilities, Keck-SEM, supported through the NSF MRSEC program (DMR-0520404).

References

(1) Choudhury, B.; Shinar, R.; Shinar, J. *J. Appl. Phys.* **2004**, *96* (5), 2949−2954.
(2) Edel, J. B.; Beard, N. P.; Hofmann, O.; DeMello, J. C.; Bradley, D. D. C.; deMello, A. J. *Lab Chip* **2004**, *4* (2), 136−140.
(3) Hofmann, O.; Wang, X. H.; deMello, J. C.; Bradley, D. D. C.; deMello, A. J. *Lab Chip* **2005**, *5* (8), 863−868.
(4) McGuinness, C. D.; Sagoo, K.; McLoskey, D.; Birch, D. J. S. *Appl. Phys. Lett.* **2005**, *86* (26).
(5) Rebohle, L.; Gebel, T.; Yankov, R. A.; Trautmann, T.; Skorupa, W.; Sun, J.; Gauglitz, G.; Frank, R. *Opt. Mater.* **2005**, *27* (5), 1055.
(6) Seo, J.; Lee, L. P. *Sens. Actuators, B* **2004**, *99* (2−3), 615−622.
(7) Misewich, J. A.; Martel, R.; Avouris, P.; Tsang, J. C.; Heinze, S.; Tersoff, J. *Science* **2003**, *300* (5620), 783−786.
(8) Holder, E.; Langeveld, B. M. W.; Schubert, U. S. *Adv. Mater.* **2005**, *17* (9), 1109−1121.
(9) Malliaras, G.; Friend, R. *Phys. Today* **2005**, *58* (5), 53−58.
(10) Bergh, A.; Craford, G.; Duggal, A.; Haitz, R. *Phys. Today* **2001**, *54* (12), 42−47.
(11) Duggal, A. R.; Foust, D. F.; Nealon, W. F.; Heller, C. M. *Appl. Phys. Lett.* **2003**, *82*, (16), 2580−2582.

(12) Slinker, J. D.; Rivnay, J.; DeFranco, J. A.; Bernards, D. A.; Gorodetsky, A. A.; Parker, S. T.; Cox, M. P.; Rohl, R.; Malliaras, G. G.; Flores-Torres, S.; Abruna, H. D. *J. Appl. Phys.* **2006**, *99* (7), 074502.
(13) Savvate'ev, V.; Chen-Esterlit, Z.; Aylott, J. W.; Choudhury, B.; Kim, C. H.; Zou, L.; Friedl, J. H.; Shinar, R.; Shinar, J.; Kopelman, R. *Appl. Phys. Lett.* **2002**, *81* (24), 4652−4654.
(14) Bernards, D. A.; Flores-Torres, S.; Abruna, H. D.; Malliaras, G. G. *Science* **2006**, *313* (5792), 1416−1419.
(15) Bernhard, S.; Barron, J. A.; Houston, P. L.; Abruna, H. D.; Ruglovksy, J. L.; Gao, X. C.; Malliaras, G. G. *J. Am. Chem. Soc.* **2002**, *124* (45), 13624−13628.
(16) Bolink, H. J.; Cappelli, L.; Coronado, E.; Gratzel, M.; Nazeeruddin, M. K. *J. Am. Chem. Soc.* **2006**, *128* (1), 46−47.
(17) Gorodetsky, A. A.; Parker, S.; Slinker, J. D.; Bernards, D. A.; Wong, M. H.; Malliaras, G. G.; Flores-Torres, S.; Abruna, H. D. *Appl. Phys. Lett.* **2004**, *84* (5), 807−809.
(18) Handy, E. S.; Pal, A. J.; Rubner, M. F. *J. Am. Chem. Soc.* **1999**, *121* (14), 3525−3528.
(19) Rudmann, H.; Shimada, S.; Rubner, M. F. *J. Am. Chem. Soc.* **2002**, *124* (17), 4918−4921.
(20) Slinker, J.; Bernards, D.; Houston, P. L.; Abruna, H. D.; Bernhard, S.; Malliaras, G. G. *Chem. Commun.* **2003**, (19), 2392−2399.
(21) Slinker, J. D.; Gorodetsky, A. A.; Lowry, M. S.; Wang, J. J.; Parker, S.; Rohl, R.; Bernhard, S.; Malliaras, G. G. *J. Am. Chem. Soc.* **2004**, *126* (9), 2763−2767.
(22) Tamayo, A. B.; Garon, S.; Sajoto, T.; Djurovich, P. I.; Tsyba, I. M.; Bau, R.; Thompson, M. E. *Inorg. Chem.* **2005**, *44* (24), 8723−8732.
(23) Kalyuzhny, G.; Buda, M.; McNeill, J.; Barbara, P.; Bard, A. J. *J. Am. Chem. Soc.* **2003**, *125* (20), 6272−6283.
(24) deMello, J. C. *Phys. Rev. B* **2002**, *66* (23), 235210.
(25) deMello, J. C.; Tessler, N.; Graham, S. C.; Friend, R. H. *Phys. Rev. B* **1998**, *57* (20), 12951−12963.
(26) Dick, D. J.; Heeger, A. J.; Yang, Y.; Pei, Q. B. *Adv. Mater.* **1996**, *8* (12), 985−987.
(27) Gao, J.; Dane, J. *Appl. Phys. Lett.* **2004**, *84* (15), 2778−2780.
(28) Pei, Q. B.; Yu, G.; Zhang, C.; Yang, Y.; Heeger, A. J. *Science* **1995**, *269* (5227), 1086−1088.
(29) Czaplewski, D.; Kameoka, J.; Craighead, H. G. *J. Vac. Sci. Technol., B* **2003**, *21* (6), 2994−2997.
(30) Kameoka, J.; Craighead, H. G. *Appl. Phys. Lett.* **2003**, *83* (2), 371−373.
(31) Kameoka, J.; Orth, R.; Yang, Y. N.; Czaplewski, D.; Mathers, R.; Coates, G. W.; Craighead, H. G. *Nanotechnology* **2003**, *14* (10), 1124−1129.
(32) Reneker, D. H.; Chun, I. *Nanotechnology* **1996**, *7* (3), 216−223.
(33) Kameoka, J.; Ilic, R.; Czaplewski, D.; Mathers, R. T.; Coates, G. W.; Craighead, H. G. *J. Photopolym. Sci. Technol.* **2004**, *17* (3), 421−425.
(34) Ko, H.; Kameoka, J. *J. Photopolym. Sci. Technol.* **2006**, *19* (3), 413−418.
(35) Bellan, L. M.; Coates, G. W.; Craighead, H. G. *Macromol. Rapid Commun.* **2006**, *27* (7), 511−515.
(36) Patel, A. C.; Li, S. X.; Yuan, J. M.; Wei, Y. *Nano Lett.* **2006**, *6* (5), 1042−1046.
(37) Fang, X.; Reneker, D. H. *J. Macromol. Sci., Phys.* **1997**, *B36* (2), 169−173.
(38) Bellan, L. M.; Cross, J. D.; Strychalski, E. A.; Moran-Mirabal, J.; Craighead, H. G. *Nano Lett.* **2006**, *6* (11), 2526−2530.
(39) Lee, S. W.; Belcher, A. M. *Nano Lett.* **2004**, *4* (3), 387−390.
(40) Dror, Y.; Salalha, W.; Khalfin, R. L.; Cohen, Y.; Yarin, A. L.; Zussman, E. *Langmuir* **2003**, *19* (17), 7012−7020.
(41) Salalha, W.; Dror, Y.; Khalfin, R. L.; Cohen, Y.; Yarin, A. L.; Zussman, E. *Langmuir* **2004**, *20* (22), 9852−9855.
(42) Liu, H. Q.; Edel, J. B.; Bellan, L. M.; Craighead, H. G. *Small* **2006**, *2* (4), 495−499.
(43) Bellan, L. M.; Kameoka, J.; Craighead, H. G. *Nanotechnology* **2005**, *16* (8), 1095−1099.
(44) Lyons, C. H.; Abbas, E. D.; Lee, J. K.; Rubner, M. F. *J. Am. Chem. Soc.* **1998**, *120* (46), 12100−12107.
(45) Rudmann, H.; Rubner, M. F. *J. Appl. Phys.* **2001**, *90* (9), 4338−4345.
(46) Hoshino, K.; Yamada, K.; Matsumoto, K.; Shimoyama, I. *J. Micromech. Microeng.* **2006**, *16* (7), 1285−1289.
(47) Jewell, J. L.; Harbison, J. P.; Scherer, A.; Lee, Y. H.; Florez, L. T. *IEEE J. Quantum Electron.* **1991**, *27* (6), 1332−1346.
(48) Granstrom, M.; Berggren, M.; Inganas, O. *Science* **1995**, *267* (5203), 1479−1481.

NL062778+